International Symposium
On Turbulence and Shear Flow
Phenomena (TSFP-9)
June 30 - July 3, 2015 *Melbourne, Australia*

OSCILLATORY FLOW IN THE HUMAN AIRWAYS FROM THE MOUTH THROUGH SEVERAL BRONCHIAL GENERATIONS

Andrew J. Banko
Department of Mechanical Engineering
Stanford University
Stanford, CA 94305, USA

Filippo Coletti
Department of Aerospace Engineering and Mechanics
University of Minnesota
Minneapolis, MN 55455, USA
fcoletti@umn.edu

Christopher J. Elkins
Department of Mechanical Engineering
Stanford University
Stanford, CA 94305, USA

John K. Eaton
Department of Mechanical Engineering
Stanford University
Stanford, CA 94305, USA

ABSTRACT

The time-varying flow is studied experimentally in an anatomically accurate model of the human airways from the mouth through several generations of bronchial branching. The airway geometry is obtained from the CT scan of a healthy adult male of normal height and build. The three-component, three-dimensional mean velocity field is obtained throughout the entire model using phase-locked Magnetic Resonance Velocimetry. A pulsatile pump drives a sinusoidal waveform (inhalation and exhalation) with frequency and stroke-length such that the mean trachea Reynolds number at peak inspiration is $Re = 4200$ and the Womersley number is $\alpha = 7$. Integral parameters are defined to quantify the degree of velocity profile non-uniformity (related to axial dispersion) and secondary flow strength (lateral dispersion), with implications drawn for the transport of particles. It is found that both parameters can vary non-trivially across successive bronchial generations, different bronchial paths, and during inhalation as compared to exhalation. They are particularly sensitive to local geometric features found in realistic anatomies, such as generation length and branching angle, and can be influenced by the moderate oscillation frequency of the bulk flow.

INTRODUCTION

The flow in the human airways spans a wide range of flow phenomena: for example merging streams, oscillating flow, turbulence, secondary flows, and separation. Understanding the integrated effect of these features in real human anatomies is critical to predicting particle transport in the respiratory system, which is important for the treatment of respiratory disease and the inhalation of airborn pollutants.

Various levels of idealization have been assumed in previous studies. Much of the prior work focused on the flow in branching tubes assembled from simple shapes and with left-to-right symmetry in both the bronchial tree and extrathoracic airways (Weibel, 1963; Stapleton *et al.*, 2000). These studies elucidated many fundamental details including secondary flow structure, acceleration through the mouth, orientation and dispersion of the laryngeal jet, and turbulent transport in the larynx (Brouns *et al.*, 2007; Shinneeb & Pollard, 2012; Kleinsteuer & Zhang, 2010). However, these models do not include realistic features such as asymmetric branching and large branching angles. As a result the topology of the flow field may be fundamentally different from real airway flows, especially in truncated models which neglect the influence of upstream airways (Choi *et al.*, 2009).

Recently, studies in anatomically accurate models have been stimulated by improvements in manufacturing technology, measurement techniques, and simulation capability. De Rochefort *et al.* (2007) used magnetic resonance velocimetry to study the steady flow in the proximal thoracic airways with comparison to simulations. Zhang *et al.* (2012) performed numerical simulations of cigarette smoke inhalation. Lambert *et al.* (2011) conducted a Large Eddy Simulation (LES) in a CT-based airway model, demonstrating left-to-right asymmetry in ventilation and particle depostion patterns.

Time-dependent flow features resulting from the inspiration/expiration cycle are noticeable even for the moderate breathing frequency associated with light activity. The effect of flow oscillation is important when the Womersley number, defined by equation 1, is greater than unity:

$$\alpha = \frac{D}{2}\sqrt{\frac{\omega}{\nu}} \tag{1}$$

D is the diameter of the airway, ω is the frequency, and ν is the kinematic viscosity. Grosse *et al.* (2007) studied time-varying flow in the upper airways using Particle Image Velocimetry (PIV) but were limited to the region around the first bifurcation. Yin *et al.* (2013) developed a patient-specific lung model with time-varying regional ventilation for use in LES. The added residence time surrounding flow reversal may increase the probability of deposition of small particles which migrate towards the walls via Brownian motion. Alternatively, extremely small particles may be subse-

quently exhaled and never deposit; a phenomenon missed by continuous flow through studies.

Understanding dispersion mechanisms and developing measures of dispersion based on a known velocity field are of interest for predicting particle transport and subsequent deposition, designing new mechanical ventilators, or interpreting bolus inhalation tests. Multiple modes of transport are important: advection by the bulk flow, longitudinal dispersion due to gradients in the streamwise velocity, lateral transport by secondary flows, disperion by turbulent motion, and Brownian diffusion. Turbulent transport is significant in the extrathoracic airways where the Reynolds number is high, and diffusion is relevant for nano-size particles. The flow is less turbulent in the first several generations of the bronchial tree, so longitudinal and lateral transport of inertial particles by the bulk flow may play a more important role. Moreover, the branching airway geometry in this region tends to promote skewed velocity profiles and secondary motion. Finally, the large inter-patient variability of deposition efficiency in studies of aerosol drug delivery suggests that realistic anatomy has important effects.

In the present paper we investigate the three-dimensional phase-averaged velocity field during inhalation and exhalation in an anatomically accurate model of the human airways from the mouth through several generations of bronchial branching. Magnetic Resonance Velocity (MRV) is used to obtain the three-component velocity field throughout the entire model volume. The specific objective of this contribution is to quantify the impact of the breathing cycle at realistic respiration frequency on flow structures and dispersion metrics derived from the velocity field in the trachea and bronchial tree. In particular, integral measures are introduced to describe both streamwise and lateral mixing.

EXPERIMENTAL METHODS

The anatomy was provided by Professor C. Kleinstreuer (North Carolina State University, NC). It was obtained from the CT-scan of a 47-year old healthy male, 174 cm in height and 78 kg in weight, with no history of respiratory disease. A General Electric 64-slice CT scanner was used to image transverse planes at a resolution of 0.97 mm x 0.97 mm with an original slice thickness of 2.5 mm. Intermediate slices were created via interpolation yielding a final slice thickness of 1.25 mm. The imaged region was from the extra-cranial skull base to the abdominal region and the data were segmented using the ScanIP software (Simpleware Inc.). The anatomy is shown in Figure 1a. The most distal bronchi in the model correspond to the eighth generation of branching, while most of the bronchial paths in the model truncate at the fifth generation.

The geometry without any scaling was used to manufacture the solid model depicted in Figure 1b by stereolithography at the University of Texas El Paso, TX. It consists of three parts flanged together: an inlet, an extrathoracic piece, and a thoracic piece. The inlet provides flow conditioning to mitigate secondary flows and develop a quasi-plug flow at the entrance to the anatomical section. The extrathoracic piece begins at the middle of the mouth; this truncation was made to avoid the influence of a specific positioning of the lips and teeth. It extends to the mid-trachea where it joins the thoracic piece, which encompases the rest of the bronchi. The terminal bronchi from each lobe of the lung exhaust into five plena, one for each lobe: right upper lobe (RUL), right middle lobe (RML), right lower lobe (RLL), left upper lobe (LUL), and left lower lobe (LLL). Each plenum is at least 20 times larger in characeristic dimension than the terminal bronchi diameters. Seperate plastic tubes connect each plenum to a reservoir. A more detailed description is given in Banko *et al.* (2015 (In Press).

Water with the addition of 0.06 mol/L of copper sulfate was used as the working fluid in order to maximize signal intensity. Dynamic similarity with the flow of air was maintained by adjusting the Reynolds number and Womersley number. The flow rate followed a sinusoidal waveform imposed by a custom volumetric pump. At peak inspiration/expiration the flow rate was 3.78 L/min with a bulk trachea velocity of $U_T = 0.22$ m/s, which is equivalent to about 60 L/min in air. This corresponds to a Reynolds number based on the trachea diameter of $Re = 4200$. The oscillation period of the flow was 10 seconds, resulting in a Womersley number of $\alpha = 7$. This regime is relevant to breathing during moderate exertion. The imposed flow rate waveform was verified using an ultrasonic flow meter (Transonic Systems Inc. TS410), and the ventilation was found to be nearly symmetric with respect to inhalation and exhalation throughout the bronchial tree. Figure 2 shows the measured waveform in terms of the trachea Reynolds number as a function of the phase in the breathing cycle, along with the ideal sinusoidal waveform. Due to the matched pressure drop in the long return tubes from the plena, each lobe of the lung received 20% of the total flow rate. The left-to-right division of the flow rate at the first bifurcation is similar to that found in previous studies of lung ventilation, although other proportions have also been reported (Briant & Cohen, 1989; Yin *et al.*, 2013). The right middle lobe is overventilated and for this reason is excluded from the discussion of the results.

Velocity data were obtained using the method of Magnetic Resonance Velocimetry (MRV, Elkins & Alley, 2007), using the data acquisition procedure described by Pelc *et al.* (1994). The experiment was performed at the Richard M. Lucas Center for Imaging using a 3 Tesla General Electric whole body scanner with an 8-channel cardiac coil. The flow loop passing through the bore of the magnet is shown in Figure 1c. Three-component phase-averaged velocity data were obtained throughout the entire model volume at a spatial resolution of 1 mm in each cartesian direction (as compared to the trachea diameter of 18 mm and the 4 mm diameter of the smallest reconstructed bronchi). The scanned volume includes both the fluid and solid model walls. Wall identification was performed via thresholding based on the signal magnitude: voxels with magnitude greater than 5 times the magnitude of the average noise were identified as fluid. The phase-locked measurements were triggered by a digital pulse passing through an ECG converter and into the ECG trigger on the MRI system. Velocity data were obtained in separate scans for the extrathoracic piece and the thoracic piece. The extrathoracic piece was measured with 12 phase bins per period. The thoracic piece was measured with parallel imaging in order to reduce scan time while maintaining the same spatial resolution as the extrathoracic piece. Details of the acquisition procedure can be found in Brau *et al.* (2008). An outer-reduction factor of 2 was used in this study. The reconstruction was done using the ARC algorithm, which is described by Beatty *et al.* (2007). Data were acquired across 10 phase bins per period. A total of 20 bins were reconstructed using linear interpolation in time for both the extrathoracic and thoracic

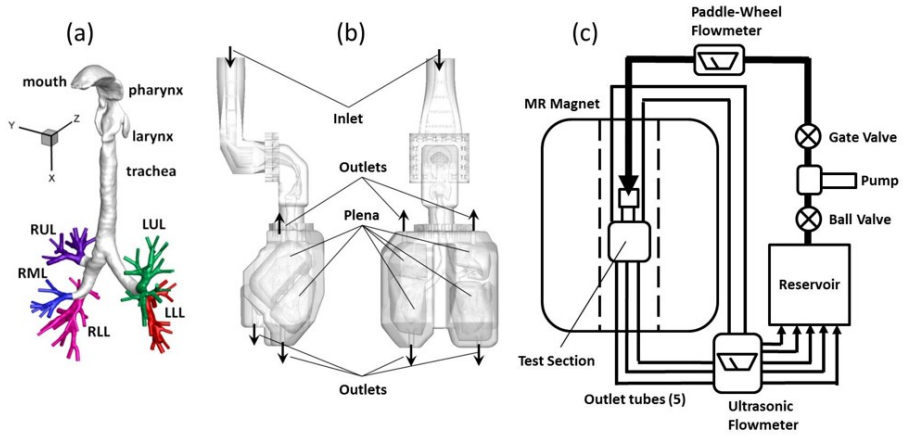

Figure 1. Global isometric view of anatomy (a), solid model manufactured using stereolithography (b), and flow loop (c).

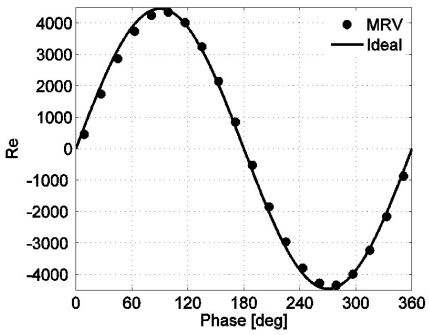

Figure 2. Measured trachea Reynolds number as a function of respiration phase with ideally imposed sinusoidal waveform.

pieces. The expected uncertainty in the MRV measurements is given by the formula of Pelc *et al.* (1994):

$$\delta_V = \frac{\sqrt{2}}{\pi} \frac{Venc}{SNR} \tag{2}$$

Venc is the velocity encoding value which controls the maximum measureable velocity free of aliasing and *SNR* is the signal to noise ratio. In the extrathoracic scan, the *Venc* was fixed at 0.6 m/s in the coronal plane, 0.7 m/s in the sagittal plane, and 1 m/s in the transverse plane. The *SNR* in this region was 32. In the thoracic scan, the *Venc* was fixed at 0.4 m/s in each direction and the *SNR* was 11. This results in an uncertainty of about 7% of the bulk velocity in the trachea at peak inspiration throughout the entire model.

RESULTS AND DISCUSSION

The full data set comprises the phase-averaged, three-component velocity at approximately 1.5×10^6 points on a uniform cartesian grid. This section first discusses qualitative features of the flow in the realistic anatomy, as compared to idealized geometries, with emphasis on the influence of flow oscillation. We then discuss quantitative measures of mixing based on integrals of the phase-averaged velocity field from the first bifurcation through the bronchial tree.

Flow Field

Figure 3 shows contours of streamwise velocity with secondary flow vectors at a plane one trachea diameter downstream of the glottis for phases surrounding peak inspiration and peak expiration. The streamwise component shows some similarity between the acceleration and deceleration phases surrounding peak inspiratory flow. During inspiration, the center of the laryngeal jet remains roughly in the same location across panels (a)-(c) of Figure 3. However, the secondary flows differ greatly during the acceleration and deceleration periods. During peak inspiration a strong single-sided streamwise swirl develops in the trachea as a result of the complex recirculation upstream in the larynx and persists down the first bifurcation, a feature not observed in studies on idealized symmetric geometries. The swirl is not yet formed in Figure 3a during acceleration, but lingers as a result of the flow inertia during deceleration as seen in Figure 3c. As a result, the secondary flows are asymmetric in time due to the inertia of the flow in this Womersley number regime. The same conclusions hold for panels (d)-(f) during expiration, although the secondary flow features are weaker due to the distance of this location from the first bifurcation.

Contours of normalized vorticity magnitude are shown in Figure 4 for a plane through the first bifurcation. There is spatial asymmetry when comparing the flow in the left and right main bronchi (based on physiological convention, the left main bronchus is on the right of the figure and the right main bronchus is on the left of the figure). Due to a tilt in the trachea, the flow during inhalation is better aligned with the right main bronchus and there is less vorticity away from the walls in this region. Conversely, the flow separates from the upper end of the left main bronchus where the radius of streamline curvature is larger and significant vorticity is shed into this generation. During exhalation the vorticity patterns are also markedly different in the two main bronchi. The short length of the right main bronchus and the high branching angle of the flow entering from the left upper lobe produces strong secondary flows in this region. In contrast, examination of the vector fields suggests that the secondary flow in the left main bronchus is mostly due to the Dean mechanism.

The flow at the first bifurcation also exhibits time asymmetry, similar to that observed upstream in the trachea. During the acceleration leading to peak inhalation, the high vorticity region along the left wall of the bifurcation is elon-

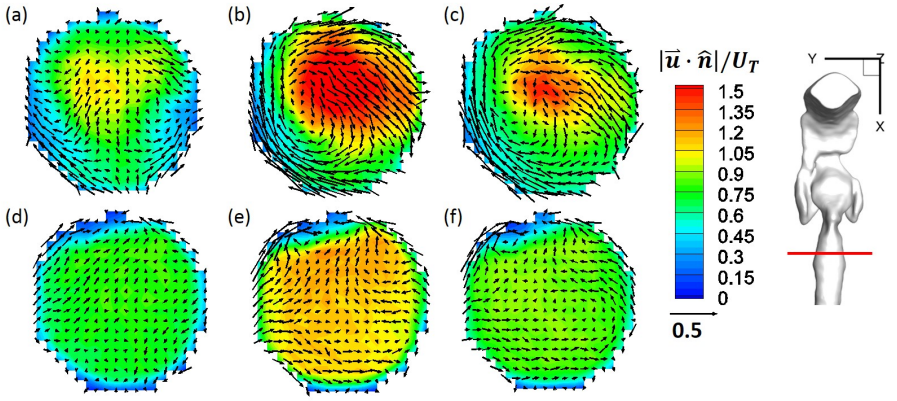

Figure 3. Streamwise velocity contours with in-plane velocity vectors, normalized by the mean speed in the trachea. Selected phases are at 45^o (a), 99^o (b), 135^o (c), 225^o (d), 279^o (e), and 315^o (f).

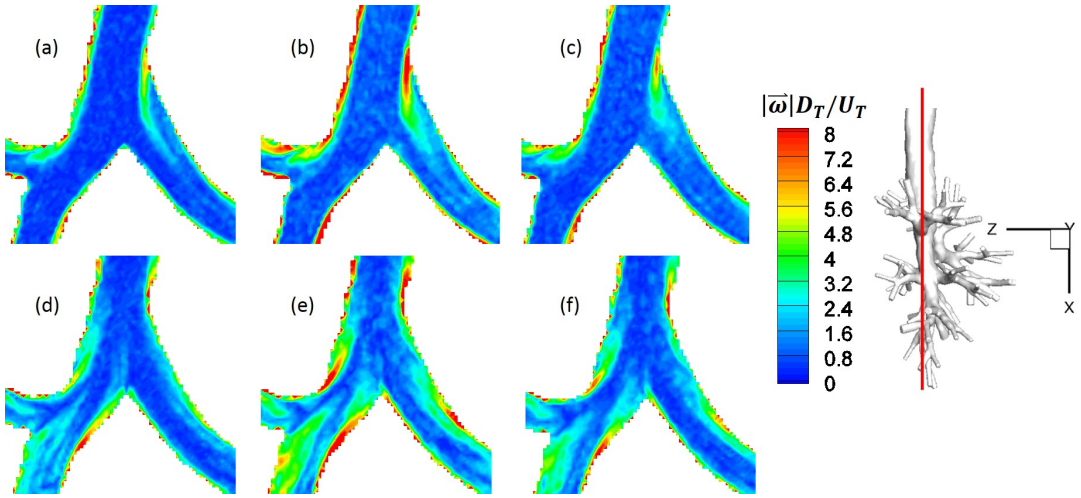

Figure 4. Contours of vorticity magnitude normalized by the mean trachea diameter and speed. Selected phases are at 45^o (a), 99^o (b), 135^o (c), 225^o (d), 279^o (e), and 315^o (f).

gated and confined along the edge of the separated region. During deceleration the high vorticity region in the same location becomes shorter and more diffuse. Therefore lateral particle dispersion by the secondary flows would likely vary across inhalation at the present Womersley number. Similarly, the vorticity distribution during exhalation becomes slightly more diffuse within the deceleration period.

Integral Parameters

In order to quantify the amount of mixing caused by the phase-averaged velocity field, we introduce integral parameters that characterize the in-plane variability of the streamwise and transverse velocities at a given cross-section of the airways. These parameters are defined as:

$$I_1 = \left(\frac{\int\int_A (\mathbf{u}\cdot\hat{\mathbf{n}})^2 \, dA}{U_T^2 A} \right)^{1/2} \tag{3}$$

$$I_2 = \left(\frac{\int\int_A (\mathbf{u} - (\mathbf{u}\cdot\hat{\mathbf{n}})\,\hat{\mathbf{n}})^2 \, dA}{U_T^2 A} \right)^{1/2} \tag{4}$$

Here $\mathbf{u}$ is the phase-averaged velocity vector, $\hat{\mathbf{n}}$ is a unit vector normal to the cross-section, A is the cross-sectional area, and U_T is the mean speed in the trachea at peak inspiration. These integral parameters describe the streamwise flow uniformity (which correlates with axial dispersion) and secondary flow strength (which correlates with lateral dispersion), respectively. The parameters calculated from the MRV measurements are plotted in Figures 5-7 for several characteristic locations. It should be noted that MRV does not resolve near wall gradients, and so I_1 will tend to be underestimated. The effect on I_2 is not as obvious. While it is expected that the no slip condition should limit the strength of near wall secondary flows, there are occasionally appreciable components in regions of reverse flow likely due to the influence of transverse pressure gradients. Also, due to the uncertainty in the measurements the approximate noise floor for the integral parameters is $I_1 \approx I_2 \approx 0.07$. The parameters are not calculated in the terminal bronchial generations due to insufficient resolution and to avoid inflow effects from the plena during exhalation.

I_1 and I_2 increase and decrease approximately in phase with the flow rate throughout the breathing cycle. As a result, both streamwise and transverse dispersion by the bulk flow should be maximum near peak inhalation and exhala-

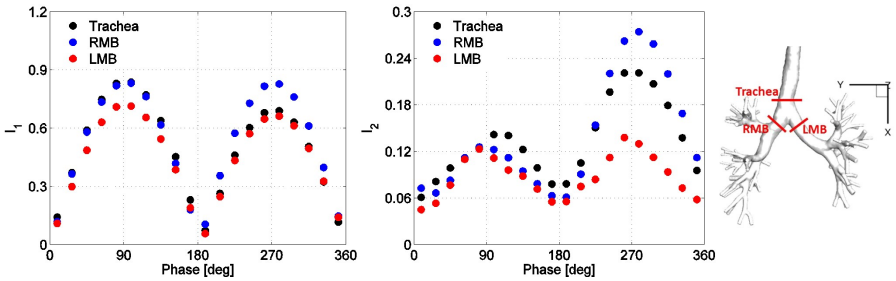

Figure 5. Integral parameters I_1 and I_2 at the first bifurcation, including the trachea, right main bronchus (RMB), and left main bronchus (LMB).

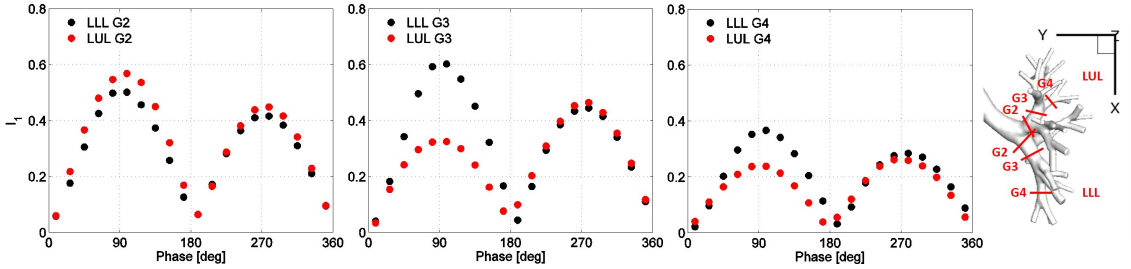

Figure 6. Integral parameter I_1 as a function of respiration phase along two bronchial paths. Nomenclature: left lower lobe (LLL), left upper lobe (LUL), generation number (G2, G3, G4).

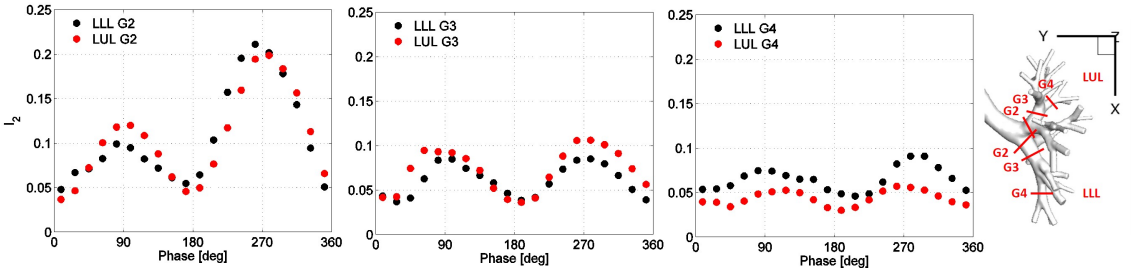

Figure 7. Integral parameter I_2 as a function of respiration phase along two bronchial paths. Nomenclature: left lower lobe (LLL), left upper lobe (LUL), generation number (G2, G3, G4).

tion as expected. The precise phase agreement varies across bronchial path and generation number suggesting that local flow features may lag or lead the variation in bulk flow rate for moderate Womersley number. This also reflects the asymmetry of secondary flows about peak inhalation and exhalation, as previously discussed.

Figure 5 plots the integral parameters in the trachea, left main bronchus, and right main bronchus. I_1 is symmetric during inhalation and exhalation for the left and right main bronchi, but decreases by about 15% in the trachea during exhalation. The merging of the flows from the two main bronchi produces a m-shaped velocity profile which has a more uniform distribution across trachea. The secondary flow strength (I_2) is symmetric in time for the left main bronchus while it increases dramatically during exhalation in the right main bronchus and trachea. The secondary flows in the right main bronchus are strongly driven by the streams merging at high branching angle from the right upper and lower lobes. Due to the short length of the right main bronchus, the circulation is carried into the lower trachea without significant decay, and dominates the weaker secondary components coming from the left main bronchus.

Figures 6 and 7 plot I_1 and I_2, respectively, along two bronchial paths. Both decrease overall from the trachea to the fourth bronchial generation; however, the progression is not necessarily monotonic and depends on the details of the local anatomy. Similarly, I_1 and I_2 do not take the same values along independent bronchial paths as shown in Figure 6, nor are they symmetric between inhalation and exhalation. Such behavior is found where the local anatomy has large branching angle, quick expansion of the cross-section, or other anatomcial features often neglected in simplified branching models. For example, I_1 at the third generation in the left lower lobe achieves a large value similar to that in the left main bronchus. The branching angle between generations two and three is large, producing a skewed velocity profile with a large value of the integral parameter.

The ratio of I_2 to I_1 represents the relative strength of secondary flow components to the streamwise component, describing the rate of transverse mixing to advection downstream. Depending non-trivially on the position in the bronchial tree and phase of the breathing cycle, this quantity can be as high as 0.5 during exhalation in generation 2 of the left lower lobe, or as low as 0.14 in the trachea and

generation 3 of the left lower lobe during inspiration.

It is difficult to draw conclusions from the integral parameters during the phases surrounding flow reversal due to the uncertainty in the velocity components. The calculated values are of the same order as the estimated root mean square noise. From examination of the vector fields, coherent secondary flow structures appear to persist through flow reversal while the streamwise component undergoes a zero crossing; however, measurements with reduced uncertainty and higher resolution in the distal bronchi are required to draw a definitive conclusion. This has possibly important implications for the continued transverse dispersion of particles during flow reversal.

CONCLUSIONS

The time-varying flow field through an anatomically accurate model of the human airways was studied at trachea based Reynolds and Womersley numbers relevant to breathing regimes during moderate exertion. Magnetic Resonance Velocimetry was used to obtain the three-dimensional, three-component phase averaged velocity field throughout the entire volume from the mouth through several generations of bronchial branching. In addition to qualitatively describing the flow features, integral parameters are defined to quantify the degree of velocity profile non-uniformity (which correlates with axial dispersion) and secondary flow strength (which correlates with lateral dispersion).

It is found that the extrathoracic airways significantly modify the tracheal flow and that the flow at the first bifurcation is highly asymmetric. Additionally, the integral measures of momentum distortion and secondary flow strength may behave non-monotonically between successive bronchial generations and can vary across independent bronchial paths. In general, this suggests that the flow in a realistic anatomy may be qualitatively different than that observed in idealized representations of the airways, with direct impact on possible measures of particle dispersion.

The effect of flow oscillation is found to produce time dependent flow features which are asymmetric with respect to the acceleration and deceleration periods surrounding peak inhalation and exhalation. The effect is most pronounced for regions of separation and on the secondary flow structure. These features are sensitive to branching angle, generation length, and other local attributes of realistic anatomies.

While the study of a single human anatomy is by definition not universal, a healthy adult male of average height and build is likely to posses more representative features than idealized models. It is imperative to understand the dependence of flow features on the real human anatomy in order to predict the flow behavior and improve medical devices such as mechanical ventilators and aerosol drug delivery systems.

REFERENCES

Banko, A.J., Coletti, F., Schiavazzi, D., Elkins, C.J. & Eaton, J.K. 2015 (In Press) Three-dimensional inspiratory flow in the upper and central human airways. *Exp. in Fluids* .

Beatty, P.J., Brau, A.C. & Chang, S. 2007 A method for autocalibrating 2-d accelerated volumetric parallel imaging with clinically practical reconstruction times. In *Proceedings of the International Society for Magnetic Resonance*, , vol. 15, p. 1749. Berlin, Germany.

Brau, A.C., Beatty, P.J., Skare, S. & Bammer, R. 2008 Comparison of reconstruction accuracy and efficiency among autocalibrating data-driven parallel imaging methods. *Magn. Reson. Med.* **59**, 382–395.

Briant, J.K. & Cohen, B.S. 1989 Flow distribution through human and canine airways during inhalation and exhalation. *J. Appl. Phys.* **67**, 1649–1654.

Brouns, M., Verbanck, S. & Lacor, C. 2007 Influence of glottic aperture on the tracheal flow. *J. Biomech.* **40**, 165–172.

Choi, J., Tawhai, M.H., Hoffman, E.A. & Lin, C.L. 2009 On intra-and intersubject variabilities of airflow in the human lungs. *Phys. Fluids* **21**, 101901.

De Rochefort, L., Vial, L., Fodil, R., Maitre, X., Louis, B. *et al.* 2007 In vitro validation of computational fluid dynamic simulation in human proximal airways with hyperpolarized ^{3}he magnetic resonance phase-contrast velocimetry. *J. Appl. Phys.* **102**, 2012–2023.

Grosse, S., Schroder, W., Klaas, M., Klockner, A. & Roggenkamp, J. 2007 Time resolved analysis of steady and oscillating flow in the upper human airways. *Exp. Fluids* **42**, 955–970.

Kleinsteuer, C. & Zhang, Z. 2010 Airflow and particle transport in the human respiratory system. *Annu. Rev. Fluid Mech.* **42**, 301–334.

Lambert, A.R., O'shaughnessy, P.T., Tawhai, M.H., Hoffman, E.A. & Lin, C.L. 2011 Regional deposition of particles in an image-based airway model: large-eddy simulation and left-right lung ventilation asymmetry. *Aerosol Science and Technology* .

Pelc, N.J., Sommer, F.G., Li, K.C.P., Brosnan, T.J., Herfkens, R.J. *et al.* 1994 Quantitative magnetic resonance flow imaging. *Magn. Reson. Q* **10**, 125–147.

Shinneeb, A.M. & Pollard, A. 2012 Investigation of the flow physics in the human pharynx/larynx region. *Exp Fluids* **53**, 989–1003.

Stapleton, K., Guentsch, E., Hoskinson, M. & Finlay, W. 2000 On the suitability of $k-\varepsilon$ modelling for aerosol deposition in the mouth and trhoat: a comparison with experiment. *J. Aerosol Sci.* **31**, 739–749.

Weibel, E.R. 1963 *Morphometry of the human lung*. New York: Academic Press.

Yin, Y., Choi, J., Hoffman, E.A., Tawhai, M.H. & Lin, C.L. 2013 A multiscale mdct image-based breathing lung model with time-varying regional ventilation. *J. Comput. Phys.* **244**, 168–192.

Zhang, Z., Kleinstreuer, C. & Hyun, S. 2012 Size-change and deposition of conventional and composite cigarette smoke particles during inhalation in a subject-specific airway model. *J. Aerosol Sci.* **46**, 34–52.